Multi-Objective Design Improvement of a Double-Stator Single-Rotor Axial Flux Brushless DC Motor with a Focus on Efficiency

Ozturk Tosun[1,*], Necibe Fusun Oyman Serteller[1], Ugur Demir[1], Onur Akar[2], Vedat Esen[3]
[1]Electric-Electronic Engineering, Faculty of Technology, Marmara University, Istanbul, Turkey
[2]Electronics and Automation, Electrononic Technologies, Marmara University, Istanbul, Turkey
[3]Electrical-Electronic Engineering, Istanbul Topkapi University, Istanbul, Turkey
[*]ozturktosun43@gmail.com; fserteller@marmara.edu.tr; udemir@marmara.edu.tr; onur.akar@marmara.edu.tr; vedatesen@topkapi.edu.tr

***Abstract*—This study comprehensively analyzes the sizing and performance optimization of a double-stator single-rotor axial flux permanent magnet brushless DC (DSSR AFPM BLDC) motor. Key design parameters, such as outer and inner diameters, slot dimensions, number of turns per phase, and phase current, were analytically determined based on the required output power, voltage, and speed. Electrical and magnetic loadings were carefully evaluated, and total losses were calculated to estimate motor efficiency. Critical parameters, including magnet thickness, air gap length, magnetic flux densities in the stator yoke and teeth, and electric loading, were optimized using genetic algorithm (GA) and ant colony optimization (ACO) techniques to maximize efficiency. These optimization processes were carried out in MATLAB. Furthermore, the motor torque and efficiency characteristics were analyzed using the finite element method (FEM). From an application perspective, this study presents novel design improvements achieved through ACO. The initial motor efficiency of 91.01 % was improved to 91.57 % using the GA method and to 91.80 % using the ACO method.**

***Index Terms*—Axial flux BLDC motor; Optimization; Genetic algorithm; Ant colony optimization.**

I. INTRODUCTION

The rise of electric vehicles has been encouraged because of their efficient operation and lower impact on environmental pollution. Research on electric vehicle technologies suggests that hybrid vehicles are more suitable [1], [2]. Considering the anticipated quantitative increase in electric cars, electrical energy consumption is essential. As fossil fuel resources diminish and their prices increase, hybrid vehicles have been developed as an alternative. Electric vehicles have rapidly gained popularity since then [3]. An electric vehicle includes mainly an electric motor, a battery system, and components for the driver. The losses from the electric motor are greater than those from the battery management system and driver semiconductor sources [4]–[6]. The losses in the electric motor consist of copper losses, core losses, friction losses, and ventilation losses. Minimizing these losses ensures the electric motor operates with high efficiency [7], [8]. Recently, the electric motors favored in the electric vehicle models produced by various brands are as follows [9]:

– Audi e-tron 55-2020: Induction motor;
– Hyundai KONA Electric-2019: Permanent magnet synchronous motor;
– Nissan Leaf SL Plus-2019: AC synchronous motor;
– Skoda CITIGOe iV-2020: Permanent magnet synchronous motor;
– BMW i3s-2020: AC synchronous motor;
– Jaguar I-Pace-2020: Permanent magnet synchronous motor;
– Opel Corsa-e-2020: AC synchronous motor;
– Kia e-Niro-2020: Permanent magnet synchronous motor;
– Tesla Model S-2022: Induction motor;
– Volkswagen ID.4-2021: Brushless DC motor;
– Volvo XC40-2021: Permanent magnet synchronous motor;
– Porsche Taycan 2020: Permanent magnet synchronous motor;
– FIAT 500e-2019: Permanent magnet synchronous motor.

The type of electric motor used in electric vehicles directly affects the efficiency and performance of the vehicle. Therefore, different types of motors are evaluated in terms of maintenance requirements and operating characteristics. Safe operation and low maintenance requirements are particularly important criteria in electric vehicle applications. In this context, the selection of the right motor plays a critical role in the success of electric vehicle systems [10]–[12]. DC motors are less favored in electric vehicle technology because of the challenges in maintaining brushes and commutators, and related maintenance costs. Induction motors are utilized in electric vehicles because of their low cost, simple

Manuscript received 9 June, 2025; accepted 14 September, 2025.

maintenance, broad speed range, and ease of manufacturing [13], [14]. However, they are less favored because of their low power density characteristics [14]. Permanent magnet synchronous motors are favored for their high efficiency, power density, compact size, high torque density, and wide speed range. These motors are classified as brushless DC (BLDC) motors due to the waveform of the flux generated in the air gap [15], [16]. In recent years, BLDC motors have been widely used in automotive, aerospace, robotics, and automation applications due to their high efficiency, torque, ease of control, and low maintenance needs. The lack of brushes and commutator components found in traditional DC motors decreases maintenance costs. Furthermore, the operational lifespan of the motor is extended [17]. When comparing the efficiency of induction motors, switched reluctance motors, DC motors, permanent magnet synchronous motors, and axial flux brushless DC (AFBLDC) motors for electric vehicles, AFBLDC motors demonstrate the most favorable performance. In terms of speed performance, both switched reluctance motors and AFBLDC motors outperform the other motor types [18]–[22]. Electric machine designers employ various optimization algorithms to achieve optimal designs, with genetic algorithms (GA) and particle swarm optimization (PSO) being the most commonly used methods. Current research focuses on optimizing efficiency, weight, and volume [23]–[26].

This article makes several key contributions to the literature as follows.

Optimization of Double-Stator AFPM BLDC Motors: This study enhances existing knowledge on high-efficiency and compact designs by focusing on a double-stator single-rotor axial flux permanent magnet (AFPM) BLDC motor. Double-stator topologies are less explored than conventional radial flux machines, making this work significant [27].

Analytical and Simulation-Based Sizing Approach: This paper outlines a thorough sizing process that integrates analytical calculations with finite element analysis (FEA) using ANSYS Environment. This method improves the accuracy and reliability of motor design predictions, which is essential for practical applications [28].

Multi-Objective Optimization Using Genetic and Ant Colony Algorithms: This study offers a comparative analysis of two nature-inspired optimization techniques, genetic algorithms (GA) and ant colony optimization (ACO), for electric motor design. This double-method approach provides valuable insight into its effectiveness in enhancing motor efficiency and decreasing volume [23].

Parameter Sensitivity Analysis: This research examines how key design parameters, such as the inner-to-outer diameter ratio and magnet thickness, affect efficiency and motor volume. This enhances the understanding of important design trade-offs in AFPM BLDC motors [24].

Validation with FEA Tools: Unlike many theoretical optimization studies, this work validates the best results obtained through simulations in Ansys Environment, ensuring practical feasibility and closing the gap between theoretical optimization and real-world applications [25].

Benchmarking Optimization Techniques: By comparing the results of GA and ACO, the study offers insights into which algorithm is more effective under particular conditions, providing guidance for future researchers and engineers focused on motor optimization [25].

This paper discusses the sizing process of a double-stator single-rotor axial flux permanent magnet (DSSR AFPM) BLDC motor. The output power, speed values, outer diameter, inner diameter, and slot dimensions are calculated analytically. The DSSR AFPM BLDC motor, designed with 12 slots and 8 poles, is modeled using the Ansys environment. Parameters like the inner-to-outer diameter ratio and magnet thickness are defined as variables in the GA. The objective function in the GA process is formulated to maximize efficiency and minimize the volume of the motor. Additionally, the ant colony optimization (ACO) algorithm is implemented in the MATLAB environment to analyze the effects of the same parameters on motor efficiency and volume. The results obtained from both optimization methods are compared accordingly. The corresponding flow diagram is shown in Fig. 1.

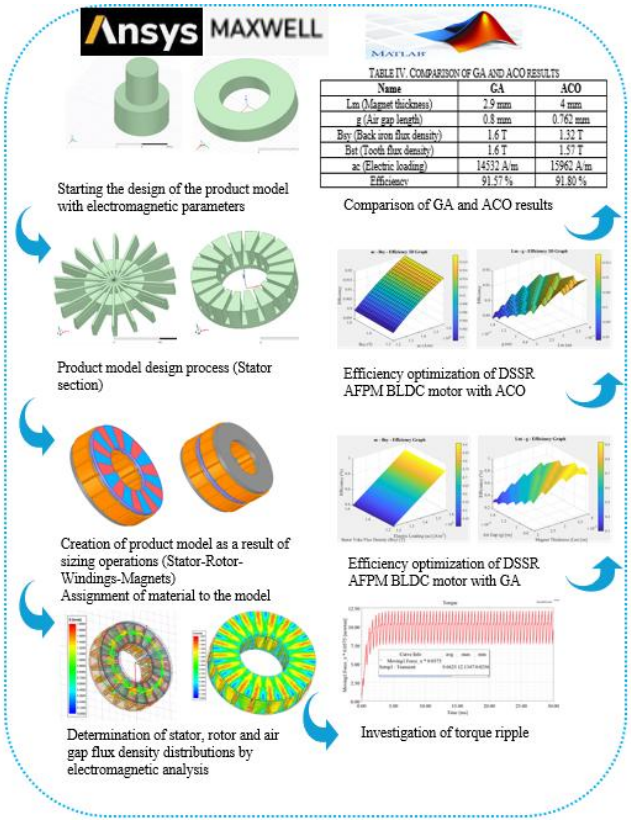

Fig. 1. The flow diagram.

This study enriches the current literature by combining analytical modeling, multi-objective optimization, and FEA-based validation for DSSR AFPM BLDC motors. It contributes to both theoretical advancements and practical design methodologies, offering a valuable resource for researchers and engineers involved in electric motor design and optimization.

II. SIZING OF DSSR AFPM BLDC MOTOR

This study performs sizing calculations for the axial flux motor based on power and speed values, while considering the boundary conditions (torque per volume). In the design of DSSR AFPM BLDC motors, electric loading and magnetic loading values constitute the initial process. The electric loading value is set at 10,000 A/m for low-power motors and 40,000 A/m for medium-power motors. The magnetic flux

density in the air gap, commonly referred to as the magnetic loading value, varies from 0.8 to 1 Tesla [29].

Figure 2 illustrates the 2D representations of the DSSR AFPM BLDC motor.

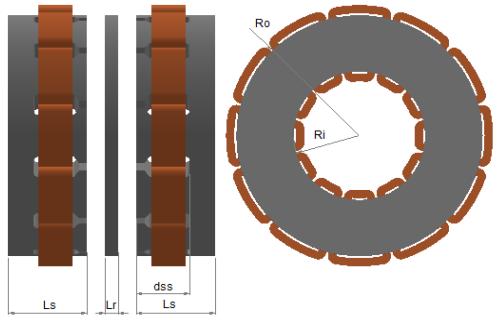

(a) (b)

Fig. 2. AFPM BLDC motor: a) Side view; b) Front view.

The output power in axial flux BLDC motors can be expressed as shown in (1)

$$P_o = 2E_{ph}I_{ph}. \tag{1}$$

The output power (P_o-W) of an axial flux motor is determined by the phase voltage (E_{ph}-V) and the phase current (I_{ph}-A)

$$E_{ph} = B_g k_w N_{ph} \omega_m DL, \tag{2}$$

where B_g is the air gap flux density (Tesla), k_w is the winding factor, N_{ph} is the number of turns per phase, ω_m is the motor speed (rpm), D is the average diameter (mm), and L is the stack length (mm). Specific electric loading (ac-A/m) and number of phase (m) are given in (3)

$$ac = mN_{ph}I_{ph\_rms} / (\pi D). \tag{3}$$

The ratio of the inner diameter to the outer diameter (K_r) of the axial flux motor is given in (4)

$$K_r = D_i / D_o. \tag{4}$$

Combining (1), (2), (3), and (4) yields the expression for the outer diameter of the axial flux motor as presented in (5)

$$D_o^3 = 12P_o / (\pi B_g k_w \omega_m ac(1-K_r^2)(1+K_r)). \tag{5}$$

Magnet poles mounted on the rotor are shown in Fig. 3.

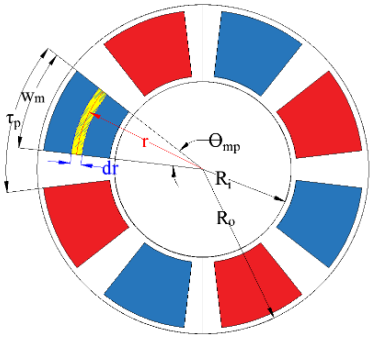

Fig. 3. The magnet poles.

The flux generated by a magnetic pole with a length of dr is expressed by (6) [30]

$$\phi(r) = \theta_{mp} B_g r dr = \alpha_i(\pi / p) B_g r dr, \tag{6}$$

where α_i is the ratio of the magnet width to the pole pitch. Magnet width (w_m) can be calculated using (7)

$$w_m = D\sin(0.5\alpha_i(360 / P)). \tag{7}$$

Half of the flux produced by the magnet pole travels through the stator yoke (Fig. 4). The total flux that passes through the stator yoke is represented by (8):

$$\phi_{bi}(r) = w_{bi} B_{sy} k_{st} dr, \tag{8}$$

$$\phi_{bi}(r) = \phi(r) / 2, \tag{9}$$

where w_{bi} (mm) is the stator yoke width, B_{sy} (Tesla) is the maximum allowable flux density in the stator yoke, and k_{st} is the lamination stacking factor of the steel material used in the stator yoke.

Figure 4 illustrates the 3D geometric view of the single-stator axial flux BLDC motor.

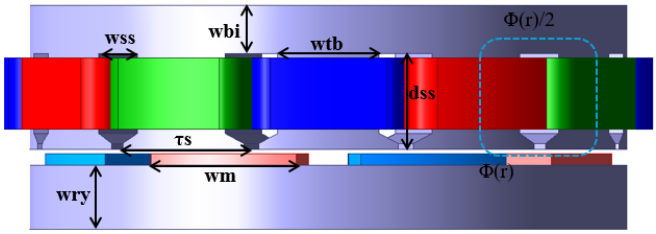

Fig. 4. The detailed parameters for the side view of AFPM BLDC motor.

When (6), (8), and (9) are combined, the width of the stator yoke, as shown in (10), can be obtained

$$w_{bi} = \alpha_i B_g \tau_{po} / (2B_{sy} k_{st}). \tag{10}$$

The width of the tooth can be described using (11)

$$w_{tb} = 2w_{bi} / N_{sm} = \alpha_i \pi B_g r / pB_{st} k_{st} N_{sm}, \tag{11}$$

where N_{sm} is the ratio of the number of motor stator slots to the number of magnet poles.

The stator tooth width reaches its minimum at the inner radius of the stator. This minimum tooth width is defined by (12)

$$w_{tbi} = \alpha_i B_g \tau_{pi} / B_{st} k_{st} N_{sm}. \tag{12}$$

The pole pitch at the inner radius of the stator is determined using (13)

$$\tau_{pi} = 2\pi R_i / P. \tag{13}$$

The slot width can be calculated using (14). It is determined by subtracting the minimum tooth width from the inner slot pitch

$$w_{ss} = \tau_{si} - w_{tbi} = (2\pi R_i / N_s) - w_{tbi}. \tag{14}$$

Copper losses (P_{cu}) are given in (15)

$$P_{cu} = mI^2_{ph\_rms}R_{ph}, \quad (15)$$

where R_{ph} is phase resistance.

Core losses (P_{core}) are generally the sum of hysteresis and eddy current losses

$$P_{core} = k_h f(B_{max})^n + k_e(fB_{max})^2, \quad (16)$$

where k_h is the hysteresis loss coefficient, k_e is the eddy current loss coefficient, f is the frequency, B_{max} is the maximum magnetic flux density, n is the material-dependent constant typically ranging between 1.6 and 2.

Inverter losses are the sum of conduction (P_{cond}) and switching losses

$$P_{cond} = mI^2_{ph\_rms}R_{on}, \quad (17)$$

where R_{on} is on-state resistance.

The switching losses (P_{sw}) can be explained by (18)

$$P_{sw} = 3V_{DC}I_{ph}f_s(t_r + t_f), \quad (18)$$

where f_s is the switching frequency and t_r and t_f are the switching rise time and switching fall time; V_{DC} is DC bus voltage.

Given the output power and losses, the efficiency (η) of the DSSR AFPM BLDC motor can be described by (19)

$$\eta = P_o / (P_o + P_{cu} + P_{core} + P_{cond} + P_{sw}). \quad (19)$$

A. Stator Design of DSSR AFPM BLDC Motor

The windings of the AFPM motor stator consist of three-phase star-connected, double-layer, concentrated windings. Concentrated windings are favored to enhance the current flowing through the conductors [2], [31]. The stator features 12 slots, and rectangular slots were selected. The rectangular section of the slots has a height of 20 mm and a width of 13.70 mm. The slot opening is 4 mm. Since there are 36 turns in each phase, the number of conductors per slot is calculated to be 18. The winding includes two parallel paths, each conductor containing five wires in the slots. The wire diameter is 1.151 mm. The winding is short-pitched, with a coil pitch of 1. M250-50A material has been used in the stator core.

Figure 5 illustrates the concentrated winding structure.

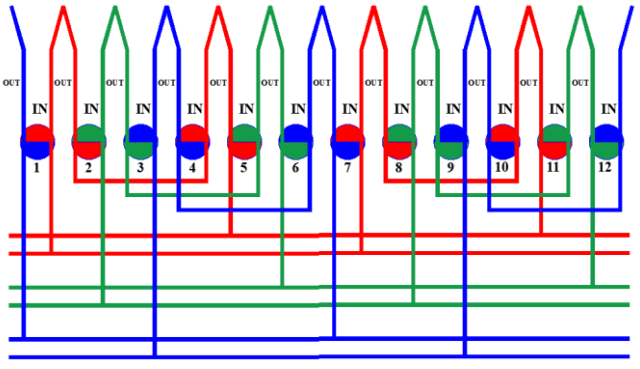

Fig. 5. The concentrated winding.

B. Rotor Design of DSSR AFPM BLDC Motor

In AFPM motors, the rotor can be designed in various configurations. The rotor core magnets can be placed as surface-mounted or embedded. The rotor core features an outer diameter of 150 mm and an inner diameter of 80 mm, with 8 magnet poles (N42H) mounted. The axial length of the motor is 8 mm, and its radial length is 28 mm. The surface-mounted magnet and interior (embedded) magnet structures are shown in Figs. 6(a) and 6(b), respectively.

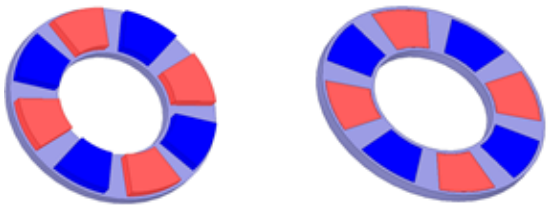

(a) (b)

Fig. 6. (a) Surface-mounted magnet; (b) Embedded magnet.

A thicker rotor core is necessary when magnets are embedded in the rotor. This decreases the power density of the motor. Nevertheless, the design of the stator remains unchanged. Since the magnets are surrounded by ferromagnetic material, the leakage flux at the edges of the magnets is greater than in surface-mounted designs. With a consistent magnet thickness and magnetization along the radius of the motor, excessive saturation in the rotor core can happen. This is because the inner radius of the fixed magnets can be relatively close to one another, depending on the machine's inner diameter and pole count [32], [33]. In the embedded design, the flux density at the outer radius is significantly lower, resulting in a non-uniform flux density distribution throughout the air gap of the motor. Surface-mounted permanent magnets behave like air and create a long air gap. In contrast, embedded magnets offer better protection against mechanical impact, wear, and corrosion, thus lowering the risk of magnet pole breakage [34]–[37].

III. Analysis of the DSSR AFPM BLDC Motor

In this section, magnetic analysis, electrical analysis, and performance parameters of the AFPM motor are conducted using ANSYS Environment. The formation of magnetic flux density in the air gap, stator, and rotor was investigated. Consequently, the saturation conditions of the chosen magnetic core material are analyzed. The speed, winding configuration, and induced voltage that influence motor performance and control are also analyzed. The status of performance parameters, such as output power, torque, efficiency, and torque ripple, is evaluated.

The specifications and dimensions of the AFPM motor are listed in Table I.

TABLE I. THE SPECIFICATIONS AND DIMENSIONS OF THE AFPM MOTOR.

Parameter	Value	Unit
Output power	5	kW
Rated speed	5000	rpm
Rated voltage	100	V
Outer diameter	150	mm
Inner diameter	80	mm
Number of slots	12	
Number of poles	8	

Parameter	Value	Unit
Embrace	0.7	
Stator axial length	36	mm
Rotor axial length	8	mm
Parallel branches	2	
Conductor per slot	18	
Number of strands	5	
Wire diameter	1.151	mm

The efficiency-speed curve is illustrated in Fig. 7.

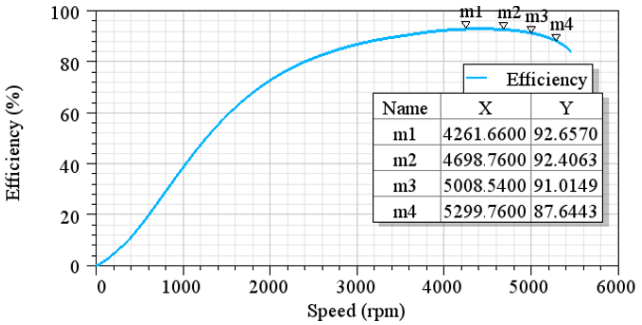

Fig. 7. Efficiency vs. speed curve.

In Fig. 7: Efficiency increases quickly at low speeds (0 rpm–1,000 rpm). In the mid-speed range (2,000 rpm–4,000 rpm), efficiency achieves high levels and stays relatively stable. The maximum efficiency is 92.6570 % at 4261.66 rpm (m1 point). At 5008.54 rpm (m3 point), the efficiency is 91.01 %, indicating a slight decrease compared to the peak efficiency. At 5299.76 rpm (m4 point), efficiency drops to 87.64 %, suggesting that high speeds result in efficiency loss.

The output torque-speed curve is presented in Fig. 8.

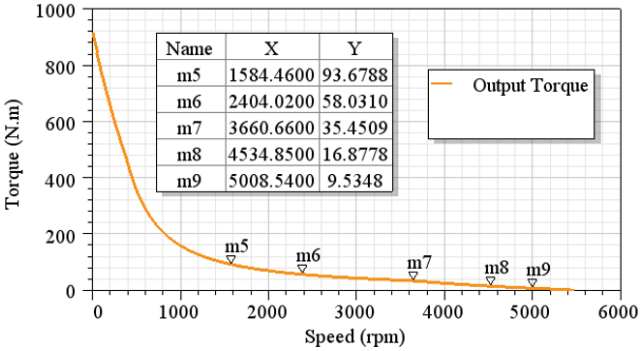

Fig. 8. The output torque-speed curve.

In Fig. 8: The torque is extremely high at low speeds (0 rpm to 1,000 rpm) (approximately 800 Nm to 900 Nm). As speed increases, torque decreases, which is expected because most electric motors exhibit a constant power characteristic: m5 point (1584 rpm, 93.67 Nm), m6 point (2404 rpm, 58.03 Nm), m7 point (3660 rpm, 35.45 Nm), m8 point (4534 rpm, 16.87 Nm), m9 point (5008 rpm, 9.53 Nm). At a speed of 5000 rpm, a torque of 9.54 Nm is produced.

The simulation results for the DSSR AFPM BLDC motor are presented in Table II.

TABLE II. THE SIMULATION RESULTS FOR THE DSSR AFPM BLDC MOTOR.

Parameter	Value	Unit
Average input current	54.92	A
Specific electric loading	14847	A/m
Current density	4.77	A/mm^2
Output power	4999.61	W
Efficiency	91.01	%
Rated speed	5008.54	rpm
Rated torque	9.532	Nm

Figure 9 illustrates the moving torque over time.

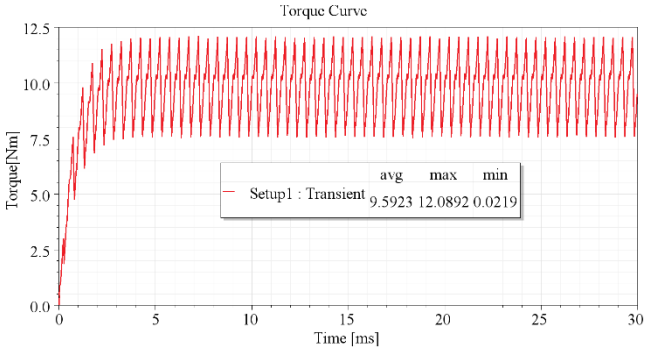

Fig. 9. The torque-speed curve during loading.

At the start (0 ms–5 ms), the torque rises rapidly before stabilizing. The average torque is 9.5923 Nm, with a maximum of 12.0892 Nm and a minimum of 0.0219 Nm. This initial rapid increase in torque indicates the starting torque of the motor. The average torque value of 9.5923 Nm reflects the efficient torque of the motor under the specified operating conditions. Torque ripple ratio ($TR\%$) is typically used to calculate torque ripple. The following formula can be used to determine this ratio

$$TR\% = ((T_{\max} - T_{\min}) / T_{avg})100. \quad (20)$$

When the torque curve is examined, it reaches a steady state after approximately 3.50 ms. At this point, the torque value is approximately 7.8 Nm. While calculating the torque ripple, the steady-state value was considered for the minimum torque. The torque ripple percentage ($TR\%$) is calculated to be approximately 44.6 %. This suggests that torque fluctuations are relatively high compared to the average torque.

The flux density is illustrated in Fig. 10.

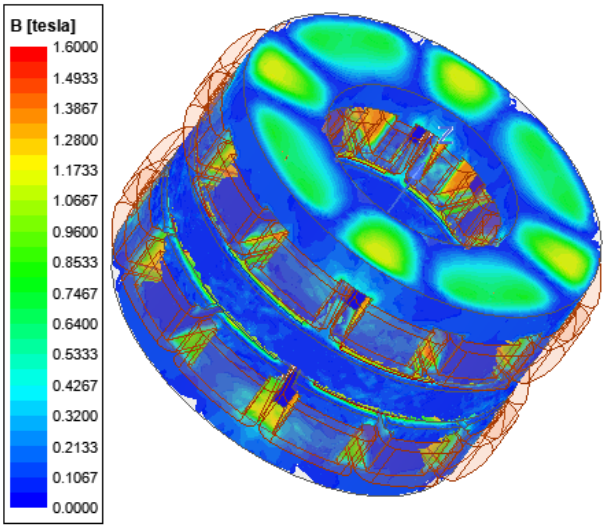

Fig. 10. The flux density.

It is observed that the maximum flux density

(approximately 1.5 T) occurs at the tooth end of the stator yoke. The average flux density in the stator teeth ranges from 1.2 T to 1.4 T. The maximum flux density in the stator yoke is 1.2 T, while the average is approximately 0.95 T. The maximum flux density in the air gap is 0.8 T, with an average of 0.5 T.

A. *Optimization of DSSR AFPM BLDC Motor Using GA*

The goal is to maximize efficiency (η) while keeping the mechanical power (Po) as close as possible to 5000 W

$$f_{\min} = -\eta + k\left|(P_o - 5000)/5000\right|. \quad (21)$$

where η, P_o, and k represent the motor efficiency, the mechanical power of the motor (W), and the penalty coefficient determining the importance of power deviation, respectively. This function ensures maximum efficiency while keeping the power close to 5000 W. If the power deviates from 5000 W, the cost function is penalized to enforce the constraint. The value ranges of the input variables are given in Table III.

Input Variables: Lm, g, Bst, Bsy, ac (given in Table III).
Objective: Maximize (η).
Constraint: $P_o \approx 5000$ W.
Penalty Function: Enforce ($P_o \approx 5000$ W).

TABLE III. INPUT VARIABLES AND THEIR VALUE RANGES.

Parameter	Value	Unit
Lm (Magnet thickness	2–4	mm
g (Air gap length)	0.75–1.5	mm
ac(Electric loading)	12–16	A/mm
Bsy (Back flux density)	1.2–1.6	T
Bst (Tooth flux density)	1.2–1.6	T

Figure 11 illustrates the ac-Bsy-efficiency graph produced by GA optimization.

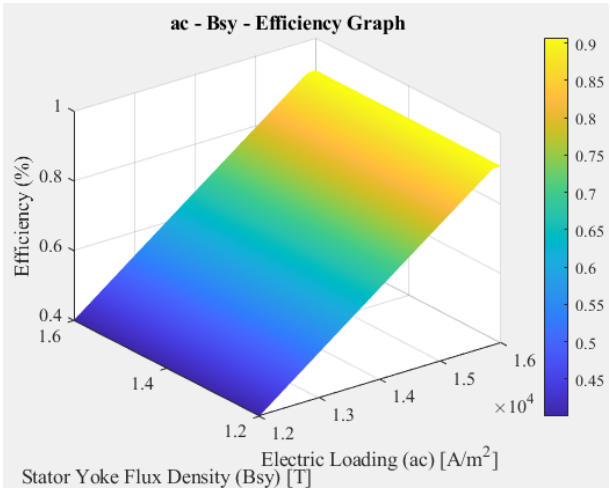

Fig. 11. Electric loading vs. stator yoke flux density vs. efficiency graph (GA).

Figure 11 illustrates the efficiency (%) of an AFPM motor based on two parameters:

– Electric Loading (ac) [A/m]: Shown on the X-axis, it represents the current density carried by the conductors of the motor.

– Stator Yoke Flux Density (Bsy) [T]: Shown on the Y-axis, it indicates the degree of magnetic saturation in the stator.

Efficiency Distribution: The surface is color-coded; blue shades signify lower efficiency (approximately 45 %), while yellow shades denote higher efficiency (around 90 %). Efficiency increases with increases in electric loading and stator flux density. The upper-right area (high AC and Bsy values) shows the highest efficiency.

Optimal Region: Low electric loading and low stator yoke flux density lead to poor efficiency. Medium to high values create the most efficient operating region.

Figure 12 illustrates the efficiency (%) of an AFPM motor as a function of magnet thickness (Lm) and air gap (g) as a result of GA optimization.

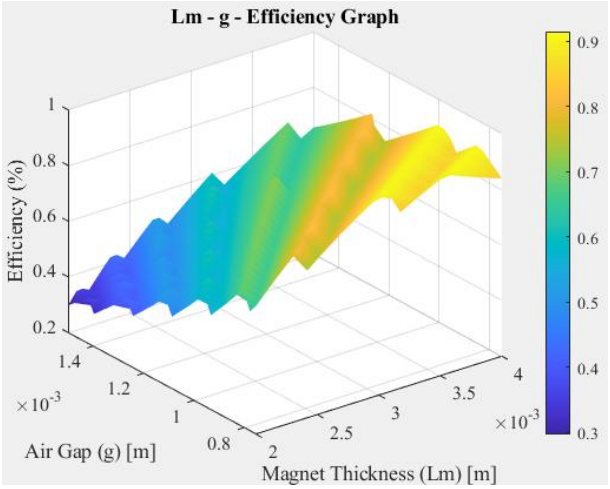

Fig. 12. Magnet thickness vs. air gap vs. efficiency graph (GA).

Efficiency Distribution: At low Lm and low g values, efficiency remains low (depicted in blue and green tones, around 30 %–50 %). As the magnet thickness increases and the air gap reaches a moderate level, efficiency improves (illustrated in yellow tones, up to ~90 %). However, efficiency can decrease again if the air gap becomes too large. Increasing magnet thickness positively influences efficiency, but excessively high Lm values may increase costs. A very small air gap negatively affects efficiency, while an excessively large gap can lead to magnetic leakage.

Figure 13 shows the optimization process of an GA.

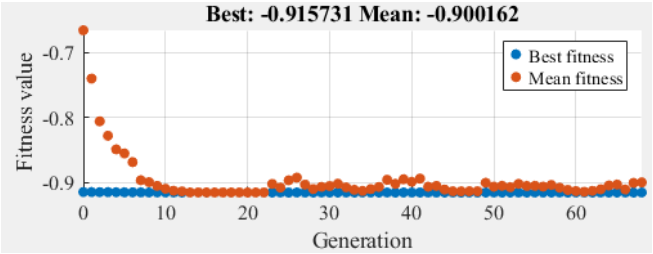

Fig. 13. Fitness value vs. GA generation curve.

Significant Changes in Early Generations: In the initial generations, both the peak and the average fitness values rise rapidly. This suggests that the genetic algorithm achieves considerable improvements at the start. Stabilization Phase: After approximately the 10th generation, the fitness values exhibit minimal changes, and the system reaches stability. The average fitness value is close to the peak fitness value, signifying decreased genetic diversity and a stabilized optimization process.

Final State:

– Best fitness value: -0.915731;

– Mean fitness value: -0.900162.

The algorithm has identified an optimal value around -0.915, with no further improvements.

B. Optimization of DSSR AFPM BLDC Motor Using ACO

The variables Lm, g, Bsy, Bst, and ac determined for the genetic algorithm were also applied in the ant colony. Similar to the genetic algorithm, the optimal values of these variables were achieved for efficiency optimization in the ant colony. Figure 14 illustrates the ac-Bsy-efficiency graph resulting from ACO optimization.

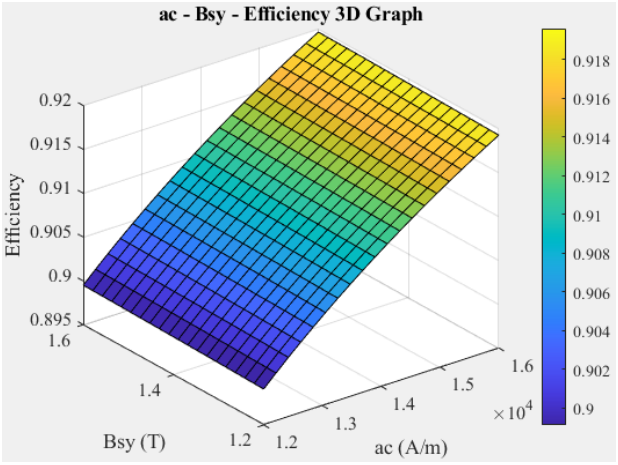

Fig. 14. Electric loading vs. stator yoke flux density vs. efficiency graph (ACO).

Efficiency Increase: As Bsy and ac increase, efficiency also increases. The lowest efficiency (~0.895) occurs at low Bsy and low ac values (bottom-left corner of the graph). The highest efficiency (~0.918) is achieved at high Bsy and high ac values (top-right corner of the graph).

Slope and Trend: The curve shows a linear increase, but may reach saturation at some point. At low Bsy and low ac values, the efficiency remains lower.

Higher Bsy and ac values result in enhanced motor efficiency. However, one must consider material limitations, saturation, and heating effects at very high values.

Figure 15 shows the Lm-g-efficiency graph as a result of ACO optimization.

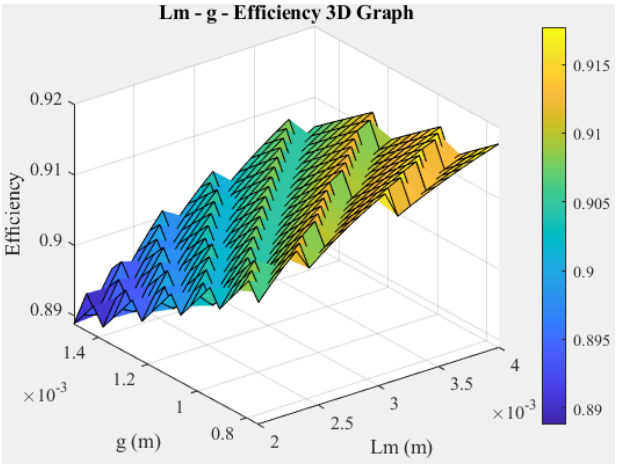

Fig. 15. Magnet thickness vs. air gap vs. efficiency graph (ACO).

Efficiency Increase: As Lm (magnet thickness) and g (air gap) increase, overall efficiency tends to improve. The lowest efficiency (~0.89) is observed at low Lm and low g values (bottom-left corner of the graph). The highest efficiency (~0.915) is seen at higher Lm and g values (top-right section of the graph).

Fluctuating Surface: The graph exhibits a fluctuating surface, indicating that there are local maximum and minimum points at specific Lm and g values.

Although efficiency generally increases with Lm and g, there are instances where it temporarily decreases. Table IV presents a comparison of GA and ACO results.

TABLE IV. INPUT VARIABLES AND THEIR VALUE RANGES.

Parameter	GA	ACO
Lm (Magnet thickness	2.9 mm	4 mm
g (Air gap length)	0.8 mm	0.762 mm
ac(Electric loading)	14532 A/m	15962 A/m
Bsy (Back flux density)	1.6 T	1.32 T
Bst (Tooth flux density)	1.6 T	1.57 T

This table compares the key design parameters of an AFPM motor optimized using a genetic algorithm (GA) and ant colony optimization (ACO). Let us analyze each parameter and the effects of the optimization methods.

ACO chose a thicker magnet, which typically enhances magnetic flux without hitting saturation. However, this might raise the cost of the magnet. ACO chose a smaller air gap, which typically enhances magnetic performance and efficiency, but necessitates greater manufacturing precision. GA achieved a higher flux density, but 1.6 T is near magnetic saturation. The ACO selection of 1.32 T offers a safer operating range. The difference is minimal, with GA generating slightly higher tooth flux density. ACO exhibits higher electric loading, which can lead to greater power output, but may also cause increased copper losses. The efficiency achieved with ACO (91.80 %) is marginally higher than that of GA (91.57 %). ACO utilized a thicker magnet and a slightly reduced air gap, leading to increased electric loading (ac).

GA exhibited a higher back iron flux density and utilized a thinner magnet for optimization.

Both methods produced comparable efficiencies (91.57 % vs. 91.80 %), with ACO showing slightly greater efficiency. If cost and manufacturing feasibility are priorities, GA may be a better choice because of its thinner magnet and larger air gap. However, ACO seems to be the superior option for higher efficiency and electrical loading.

IV. DISCUSSION

In this section, an axial flux BLDC motor design optimized using a genetic algorithm (GA) in MATLAB was validated using the RMxprt module of ANSYS. The maximum efficiency obtained from the MATLAB-based optimization was 91.57 %, while the same design parameters yielded a 91.71 % efficiency in RMxprt. The 0.14 % difference is negligible from an engineering standpoint and confirms the validity of the optimization approach.

Additionally, as shown in Table V, the comparison of key performance parameters between MATLAB and RMxprt reveals a high level of consistency. Parameters such as electric loading (14532 A/m vs. 14694 A/m) and tooth flux density (1.6 T vs. 1.50 T) differ by less than 5 %, indicating

that the analytical model offers a reliable estimation of magnetic loading.

A more notable difference is observed in the back iron flux density (1.6 T in MATLAB vs. 1.30 T in RMxprt), with approximately 18 % deviation. This can be attributed to the linear material assumptions used in the MATLAB model, which does not fully capture magnetic saturation. In contrast, RMxprt represents the magnetic circuit in greater detail, providing more realistic results.

The rated torque (9.54 Nm vs. 9.78 Nm) and rated speed (5000 rpm vs. 4877 rpm) values are also in close agreement, confirming that the optimized design successfully meets the target performance.

In conclusion, the GA-assisted MATLAB model provides an effective and practical method for motor pre-design and rapid optimization. The RMxprt validation reinforces its reliability and engineering applicability.

Table V compares the MATLAB-GA and ANSYS RMxprt results.

TABLE V. MATLAB-GA AND ANSYS RMxprt RESULTS.

Parameter	MATLAB-GA	RMxprt
Electric loading	14532 A/m	14694 A/m
Back flux density	1.6 T	1.30 T
Tooth flux density	1.6 T	1.50 T
Rated torque	9.54 Nm	9.78 Nm
Rated speed	5000 rpm	4877 rpm

An axial flux BLDC motor design optimized using the ant colony optimization (ACO) algorithm in MATLAB was validated through RMxprt simulations in ANSYS. The maximum efficiency obtained through MATLAB simulations was 91.80 %, while the corresponding RMxprt analysis yielded an efficiency of 91.65 %.

The difference between the two results is only 0.15 %, which is negligible from an engineering perspective. This close agreement confirms the accuracy and reliability of the ACO-based optimization approach. The design proposed by the ACO algorithm was largely validated by RMxprt, a well-established industrial analysis tool.

As shown in Table VI, the key electromagnetic parameters - particularly tooth flux density (1.57 T vs. 1.59 T) and rated torque (9.55 Nm vs. 10.06 Nm) - show close alignment, demonstrating that the ACO algorithm effectively explores the design space and produces physically valid solutions.

However, noticeable deviations are observed in the back iron flux density (1.32 T vs. 1.12 T) and electric loading (15962 A/m vs. 14321 A/m), with differences of approximately 15 % and 10 %, respectively. These differences can be attributed to simplified linear material assumptions and limited loss modeling in the MATLAB environment. RMxprt, on the other hand, accounts for nonlinear magnetic saturation, hysteresis, and eddy current losses, providing more realistic performance estimations.

In conclusion, the ACO-assisted MATLAB model offers a fast and effective method for motor pre-design and optimization. The RMxprt validation demonstrates that the approach is not only theoretically sound, but also applicable to real-world engineering tasks.

Table VI compares the MATLAB-ACO and ANSYS RMxprt results.

TABLE VI. MATLAB-ACO AND ANSYS RMXPRT RESULTS.

Parameter	MATLAB-ACO	RMxprt
Electric loading	15962 A/m	14321 A/m
Back flux density	1.32 T	1.12 T
Tooth flux density	1.57 T	1.59 T
Rated torque	9.55 Nm	10.06 Nm
Rated speed	5000 rpm	4745 rpm

V. CONCLUSIONS

This study involved the design and optimization of a double-stator single-rotor axial flux permanent magnet brushless direct current (DSSR AFPM BLDC) motor using the genetic algorithm (GA) and ant colony optimization (ACO). The key parameters of the motor, such as magnet thickness, air gap length, stator yoke flux density, tooth flux density, and electric loading, were optimized to maximize efficiency. The optimized designs were simulated using ANSYS software, and their performance was evaluated through the finite element method (FEM).

The comparison between GA and ACO showed that ACO chose a thicker magnet and a smaller air gap, resulting in higher electric loading and a slightly improved efficiency of 91.80 % compared to GA's 91.57 %. On the other hand, GA led to a higher back iron flux density and used a thinner magnet, which could be beneficial in terms of material costs and manufacturing feasibility. While both optimization methods yielded similar efficiency values, ACO showed a slight edge in performance, whereas GA may be more suitable for cost-sensitive applications.

The results show that both GA and ACO can effectively optimize the DSSR AFPM BLDC motor. The selection of these methods relies on specific design priorities, including efficiency, cost, and manufacturing constraints. Future research can emphasize integrating multi-objective optimization techniques to achieve an optimal trade-off among efficiency, cost, and volume reduction, while further enhancing the design for industrial applications.

CONFLICTS OF INTEREST

The authors declare that they have no conflicts of interest.

REFERENCES

[1] T. E. Hajji, S. Hlioui, F. Louf, M. Gabsi, G. Mermaz-Rollet, and M. Belhadi, "Optimal design of high-speed electric machines for electric vehicles: A case study of 100 kW V-shaped interior PMSM", *Machines*, vol. 11, no. 1, p. 57, 2023. DOI: 10.3390/machines11010057.

[2] A. N. Kumar and A. Dheepanchakkravarthy, "Design and analysis of interior buried permanent magnet synchronous motor for electric vehicle applications", *Advances in Electrical and Computer Engineering*, vol. 23, no. 4, pp. 3–14, 2023. DOI: 10.4316/AECE.2023.04001.

[3] A. San, "Electric propulsion vehicle modelling and simulation", M.S. thesis, Institute of Science and Technology, Istanbul Technical University, 2011.

[4] Y. P. Yang, J.-P. Wang, S.-W. Wu, and Y.-P. Luh, "Design and control of axial-flux brushless DC wheel motors for electric vehicles-Part II: Optimal current waveforms and performance test", *IEEE Transactions on Magnetics*, vol. 40, no. 4, pp. 1883–1891, 2004. DOI: 10.1109/TMAG.2004.828165.

[5] H. Qi, L. Ling, and Z. Liwei, "Design and research of axial flux permanent magnet motor for electric vehicle", in *Proc. of 2019 IEEE 3rd International Electrical and Energy Conference (CIEEC)*, 2019, pp. 1918–1923. DOI: 10.1109/CIEEC47146.2019.CIEEC-2019658.

[6] A. E. Aliasand and F. T. Josh, "Selection of motor foran electric vehicle: A review", *Materials Today: Proceedings*, vol. 24, part 3, pp.

1804–1815, 2020. DOI: 10.1016/j.matpr.2020.03.605.
[7] H. Abdullah, G. Ramasamy, K. Ramar, and C. V. Aravind, "Design consideration of dual axial flux motor for electric vehicle applications", in *Proc. of 2015 IEEE Conference on Energy Conversion (CENCON)*, 2015, pp. 72–77. DOI: 10.1109/CENCON.2015.7409516.
[8] C. Lucas, "Weight reduction in electric motors: Aluminum vs copper wires", M.S. thesis, University of Windsor, Canada, 2020.
[9] M. A. Pastorelli, "Design of axial flux motors for automotive purpose", M.S. thesis, University of Politecnico di Torino, 2022.
[10] A. H. Isfahani and S. Sadeghi, "Design of a permanent magnet synchronous machine for the hybrid electric vehicle", *International Journal of Electrical, Electronic and Communication Sciences*, vol. 2, no. 9, pp. 1876–1880, 2008.
[11] M. Akar, M. Eker, and F. Akın, "BLDC motor design and application for light electric vehicle", *Afyon Kocatepe Üniversitesi Fen Ve Mühendislik Bilimleri Dergisi*, vol. 21, no. 2, pp. 326–336, 2021. DOI: 10.35414/akufemubid.889877.
[12] M. Ehsani, Y. Gao, S. E. Gay, and A. Emadi, *Modern Electric, Hybrid Electric, and Fuel Cell Vehicles*, 3rd ed. CRC Press, 2018, pp. 13–18. DOI: 10.1201/9781420054002.
[13] T. Raminosoa *et al.*, "Test results for a high temperature non-permanent-magnet traction motor", *IEEE Transactions on Industry Applications*, vol. 53, no. 4, pp. 3496–3504, 2017. DOI: 10.1109/TIA.2017.2687870.
[14] Y. Yang *et al.*, "Design and comparison of interior permanent magnet motor topologies for traction applications", *IEEE Transactions on Transportation Electrification*, vol. 3, no. 1, pp. 86–97, 2017. DOI: 10.1109/TTE.2016.2614972.
[15] M. Alani, Y. Öner, and A. Tameemi, "Electrical machines in automotive: Evaluation of current technologies and future requirements", *Electrical Engineering*, vol. 105, no. 1, pp. 477–491, 2023. DOI: 10.1007/s00202-022-01673-7.
[16] C. P. Priyanka and G. Jagadanand, "Design and analysis of BLDC motor for electric vehicle application", in *Advances in Automation, Signal Processing, Instrumentation, and Control. i-CASIC 2020. Lecture Notes in Electrical Engineering*, vol. 700. Springer, Singapore, 2021, pp. 977–985. DOI: 10.1007/978-981-15-8221-9_91.
[17] B. Ale, "Modeling and performance analysis of an in-wheel permanent magnet brushless DC (PM BLDC) motor in MATLAB", *Applications of Modelling and Simulation*, vol. 6, pp. 150–157, 2022. [Online]. Available: https://arqiipubl.com/ojs/index.php/AMS_Journal/article/view/372
[18] K. T. Chau, *Electric Vehicle Machines and Drives Design, Analysis and Application*. John Wiley & Sons, Hoboken, 2015, pp. 39–68. DOI: 10.1002/9781118752555.
[19] R. Bhattacharjee, "Switched reluctance motor applications to EV and HEV: Torque control issues", in *Proc. of 2014 1st International Conference on Non Conventional Energy*, 2014, pp. 324–328. DOI: 10.1109/ICONCE.2014.6808735.
[20] N. A. Rahim, H. W. Ping, and M. Tadjuddin, "Design of an in-wheel axial flux brushless DC motor for electric vehicle", in *Proc. of 2006 International Forum on Strategic Technology*, 2006, pp. 16–19. DOI: 10.1109/IFOST.2006.312234.
[21] A. N. Patel, "Slot opening displacement technique for cogging torque reduction of axial flux brushless DC motor for electric two-wheeler application", *Electrical Engineering & Electromechanics*, vol. 2023, no. 2, pp. 7–13, 2023. DOI: 10.20998/2074-272X.2023.2.02.
[22] E. Yesilbag, Y. Ertugrul, and L. Ergene, "Axial flux PM BLDC motor design methodology and comparison with a radial flux PM BLDC motor", *Turkish Journal of Electrical Engineering and Computer Sciences*, vol. 25, no. 4, pp. 3455–3467, 2017. DOI: 10.3906/elk-1611-23.
[23] A. N. Patel and B. N. Suthar, "Design optimization of axial flux surface mounted permanent magnet brushless DC motor for electrical vehicle based on genetic algorithm", *International Journal of Engineering, Transactions A: Basics*, vol. 31, no. 7, pp. 1050–1056, 2018. DOI: 10.5829/ije.2018.31.07a.07.
[24] A. Gu, B. Ruan, W. Cao, Q. Yuan, Y. Lian, and H. Zhang, "A general SVM-based multi-objective optimization methodology for axial flux motor design: YASA motor of an electric vehicle as a case study", *IEEE Access*, vol. 7, pp. 180251–180257, 2019. DOI: 10.1109/ACCESS.2019.2958088.
[25] M. A. Darmani and H. Hooshyar, "Optimal design of axial flux permanent magnet synchronous motor for electric vehicle applications using GA and FEM", *Journal of Electrical and Computer Engineering Innovations (JECEI)*, vol. 3, no. 2, pp. 89–97, 2015. DOI: 10.22061/jecei.2016.401.
[26] J. F. Gieras, R.-J. Wang, and M. J. Kamper, *Axial Flux Permanent Magnet Brushless Machines*, 2nd ed. Netherlands, Springer, 2008. DOI: 10.1007/978-1-4020-8227-6.
[27] C. Corey, "Single rotor, dual stator axial flux permanent magnet motor design, analysis and test", M.S. thesis, University of Wisconsin-Madison, 2019.
[28] M. Amin, S. Kahourzade, N. Abd Rahim, W. P. Hew, and M. N. Uddin, "Design, analysis, and prototyping of a novel-structured solid-rotor-ringed line-start axial-flux permanent-magnet motor", *IEEE Transactions on Industrial Electronics*, vol. 61, no. 4 pp. 1722–1734, 2014. DOI: 10.1109/TIE.2013.2266082.
[29] F. Sahin, "Design and development of a high-speed axial-flux permanent-magnet machine", Ph.D. dissertation, Technische Universiteit Eindhoven, 2001.
[30] N. Trong Duy, "Dual air-gap axial flux permanent magnet machines for flywheel energy storage systems", Ph.D. dissertation, Nanyang Technological University, 2012.
[31] S. A. Gholamian, M. T. A. Ablouie, A. Mohseni, and S. E. Jafarabadi, "Effect of air gap on torque density for double-sided axial flux slotted permanent magnet motors using analytic and FEM evaluation", *Journal of Applied Sciences Research*, vol. 5, no. 9, pp. 1230–1238, 2009.
[32] A. K. Sawhney, *A Course in Electrical Machine Design*. Dhanpat Rai and Corporation, 2016, pp. 3.41–3.62.
[33] M. Aydin, H. Surong, and T. A. Lipo, "Torque quality and comparison of internal and external rotor axial flux surface-magnet disc machines", *IEEE Transactions on Industrial Electronics*, vol. 53, no. 3, pp. 822–830, 2006. DOI: 10.1109/TIE.2006.874268.
[34] F. Marignetti, V. D. Colli, and S. Carbone, "Comparison of axial flux PM synchronous machines with different rotor back cores", *IEEE Transactions on Magnetics*, vol. 46, no. 2, pp. 598–601, 2010. DOI: 10.1109/TMAG.2009.2034021.
[35] C.-T. Liu, S.-C. Lin, and T.-S. Chiang, "On the analytical flux distribution modeling of an axial-flux surface-mounted permanent magnet motor for control applications", *Journal of Magnetism and Magnetic Material*, vol. 282, pp. 346–350, 2004. DOI: 10.1016/j.jmmm.2004.04.081.
[36] F. Caricchi, F. Crescimbini, and E. Santini, "Basic principle and design criteria of axial-flux PM machines having counterrotating rotors", *IEEE Transactions on Industry Applications*, vol. 31, no. 5, pp. 1062–1068, 1995. DOI: 10.1109/28.464520.
[37] O. Tosun, N. F. O. Serteller, and G. Yalcin, "Comprehensive design and optimization of brushless direct current motor for the desired operating conditions", in *Proc. of 2021 25th International Conference Electronics*, 2021, pp. 1–6. DOI: 10.1109/IEEECONF52705.2021.9467459.